





A high-affinity cocaine binding site associated with the brain acid soluble protein 1

Maged M. Harraz^{a,1}, Adarsha P. Malla^{a,2}, Evan R. Semenza^{a,2}, Maria Shishikura^a, Manisha Singh^a, Yun Hwang^a, In Guk Kang^a, Young Jun Song^a, Adele M. Snowman^a, Pedro Cortés^a, Senthilkumar S. Karuppagounder^{b,c}, Ted M. Dawson^{a,b,c,d}, Valina L. Dawson^{a,b,c,e} , and Solomon H. Snyder^{a,d,f,1} 

Contributed by Solomon H. Snyder; received January 11, 2022; accepted March 1, 2022; reviewed by Joseph Coyle and S. Enna

Cocaine exerts its stimulant effect by inhibiting dopamine (DA) reuptake, leading to increased dopamine signaling. This action is thought to reflect the binding of cocaine to the dopamine transporter (DAT) to inhibit its function. However, cocaine is a relatively weak inhibitor of DAT, and many DAT inhibitors do not share cocaine's behavioral actions. Further, recent reports show more potent actions of the drug, implying the existence of a high-affinity receptor for cocaine. We now report high-affinity binding of cocaine associated with the brain acid soluble protein 1 (BASP1) with a dissociation constant (K_d) of 7 nM. Knocking down BASP1 in the striatum inhibits [³H]cocaine binding to striatal synaptosomes. Depleting BASP1 in the nucleus accumbens but not the dorsal striatum diminishes locomotor stimulation in mice. Our findings imply that BASP1 is a pharmacologically relevant receptor for cocaine.

cocaine | BASP1 | drug abuse | receptor | behavior

Cocaine is a behavioral stimulant with substantial abuse potential related to its rewarding actions (1, 2). Cocaine inhibits the reuptake inactivation of neurotransmitters such as dopamine (DA), serotonin, and norepinephrine at high nanomolar to low micromolar concentrations (2). There is evidence for substantially more potent influences of cocaine. For instance, Calligaro and Eldefrawi reported binding of [³H]cocaine to brain membranes with a dissociation constant (K_d) of about 16 nM (3). At 10 nM concentration, cocaine elicits environmental place conditioning in planarians (4), while 1 nM cocaine enhances dopamine D2 receptor agonist-mediated signaling (5). Inhibition of the monoamine transporters by cocaine is substantially less potent than these high-affinity actions. Thus, evidence for a high-affinity receptor for cocaine that mediates its behavioral actions has been lacking.

Strategies to identify targets of small molecule ligands include genetic (6), computational (7), and biochemical (8) approaches. A typical biochemical method relies on affinity purification by immobilizing small molecule ligands as bait on solid supports. Reconstitution of the ligand-receptor complex is performed *ex vivo* by running tissue/cell lysates on small molecule affinity columns. After washing unbound material, high concentrations of the small molecule elute bound proteins, whose identity is determined by mass spectrometry. We modified this approach to preserve the native environment for ligand-receptor interaction by binding the ligand to its target(s) in live cells. Following cell lysis, ligand-receptor complexes were isolated by immunoprecipitation.

Results

Identification of Cocaine Binding Proteins. To validate our approach, we pulled down cocaine binding proteins using an antibody against cocaine. We overexpressed the wild-type dopamine transporter (WT-DAT) or L104V-F105C-A109V triple mutant DAT in HEK 293 cells. This mutant was previously reported to be insensitive to cocaine (9, 10). We incubated cocaine with live cells, then performed the pull-down experiment. Anticocaine immunoprecipitation (IP) pulls down WT-DAT but not the L104V-F105C-A109V triple mutant DAT only in the presence of cocaine (Fig. 1*A*). We treated primary cortical neuronal (PCN) cultures with 100 nM cocaine. We incubated the lysates with cocaine antibodies to identify cocaine binding proteins, which were eluted with 10 nM cocaine (Fig. 1*B*). Mass spectrometric analysis reveals six mouse proteins pulled down following treatment with cocaine but not saline. To exclude common contaminants, we checked the frequency of finding these proteins in the Contaminant Repository for Affinity Purification (CRAPome) (11) database. Beta-actin seems to be a nonspecific finding, since its maximum number of spectra and the frequency of its occurrence across 411 experiments are very high (*SI Appendix, Fig. S1 A and B*). We prioritized the brain acid soluble protein 1 (BASP1) as a putative receptor for cocaine, because it is the only

Significance

Cocaine is a monoamine transport inhibitor. Current models attributing pharmacologic actions of cocaine to inhibiting the activity of the amine transporters alone failed to translate to the clinic. Cocaine inhibition of the dopamine, serotonin, and norepinephrine transporters is relatively weak, suggesting that blockade of the amine transporters alone cannot account for the actions of cocaine, especially at low doses. There is evidence for significantly more potent actions of cocaine, suggesting the existence of a high-affinity receptor(s) for the drug. Identifying and characterizing such receptors will deepen our understanding of cocaine pharmacologic actions and pave the way for therapeutic development. Here we identify a high-affinity cocaine binding site associated with BASP1 that is involved in mediating the drug's psychotropic actions.

Reviewers: J.C., Harvard University; and S.J.E., The University of Kansas Medical Center.

The authors declare no competing interest.

Copyright © 2022 the Author(s). Published by PNAS. This article is distributed under Creative Commons Attribution-NonCommercial-NoDerivatives License 4.0 (CC BY-NC-ND).

¹To whom correspondence may be addressed. Email: ssnyder@jhmi.edu or mharraz@jhmi.edu.

²A.P.M. and E.R.S. contributed equally to this work.

This article contains supporting information online at <http://www.pnas.org/lookup/suppl/doi:10.1073/pnas.2200545119/-/DCSupplemental>.

Published April 11, 2022.

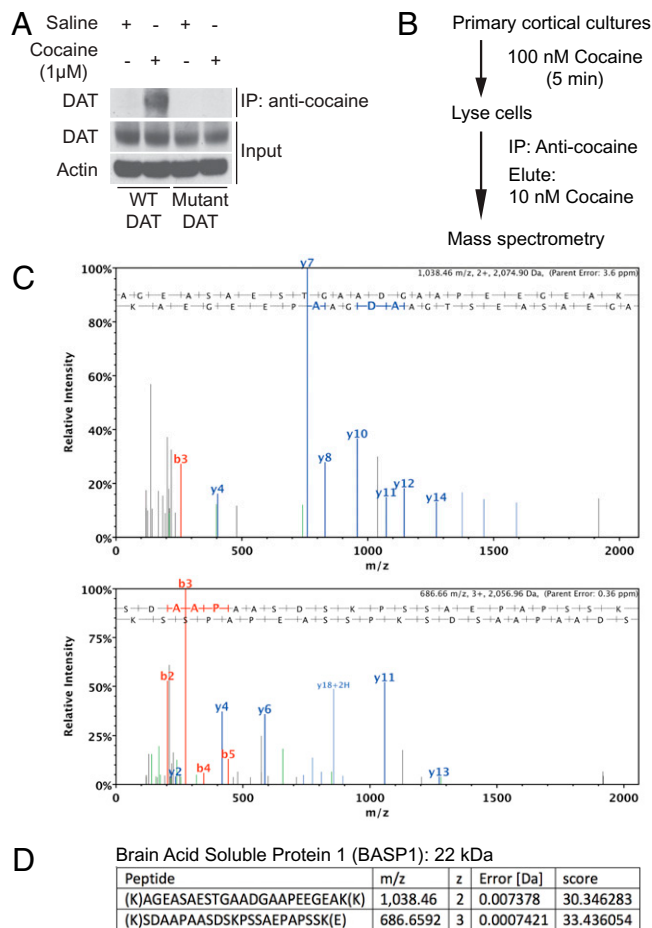


Fig. 1. Identification of cocaine binding proteins. (A) Western blot of DAT overexpressed in HEK 293 cells following IP with anti-cocaine antibody. Input of DAT and actin from the same sample used in IP serve as loading controls. L104V-F105C-A109V triple mutant DAT is insensitive to cocaine. (B) Schematic diagram of the protocol used to identify cocaine binding proteins. (C and D) MS/MS spectra of the peptides used to identify the brain acid soluble protein 1 (BASP1) in anti-cocaine immunoprecipitates.

membrane-associated protein in our results (Fig. 1 C and D and *SI Appendix, Fig. S1C*) (12–16). BASP1 does not seem to be a common contaminant in affinity pull-down/mass spectrometry experiments, since its relatively low frequency of occurrence is mostly associated with FLAG tag and magnetic beads (*SI Appendix, Fig. S1D and E*). We validated a BASP1 antibody to recognize endogenous and overexpressed BASP1 protein selectively (*SI Appendix, Fig. S1F*).

High-Affinity Cocaine Binding Associated with BASP1. We characterized the binding of [3 H]cocaine to BASP1 protein. [3 H]cocaine binds overexpressed BASP1 with high affinity, a K_d value of 7 nM (Fig. 2 A and B and *SI Appendix, Fig. S2A*). [3 H]cocaine binds to rat striatal synaptosomal fractions with a similar K_d of about 7.9 nM (Fig. 2C). The binding of [3 H]cocaine to rat striatal synaptosomes appears to involve BASP1, as depletion of BASP1 by shRNA to about 50% of control levels elicits a 50% decrease in the Bmax of [3 H]cocaine binding (*SI Appendix, Fig. S2B and C*). Depleting BASP1 protein by shRNA treatment diminishes the Bmax without influence on the K_d of [3 H]cocaine binding. Similarly, in mouse striatal synaptosomal fractions, depleting BASP1 inhibits [3 H]cocaine binding (Fig. 2 D and E). The decrease of BASP1 protein by shRNA treatment corresponds closely to the reduction of [3 H]cocaine binding. Hence, a 50% reduction in BASP1 protein levels by shRNA leads to a 50%

reduction in [3 H]cocaine binding in striatal synaptosomes. Taken together, our findings indicate that endogenous BASP1 is responsible for the great majority of high-affinity [3 H]cocaine binding in striatal synaptosomes (Fig. 2 C–E).

Dopaminergic Neurons Contribution to High-Affinity [3 H]Cocaine Binding in the Striatum. Many reports demonstrate that disruption of dopaminergic terminals in the nucleus accumbens (NAc) abolishes the locomotor activity and reinforcing actions of cocaine (17–20).

We examined the contribution of dopaminergic nerve terminals to high-affinity [3 H]cocaine binding in striatal synaptosomes. We elicited dopaminergic denervation of the striatum using a systemic injection of 1-methyl-4-phenyl-1,2,3,6-tetrahydropyridine (MPTP) (Fig. 3A), a neurotoxin, which is selectively taken up by dopaminergic neurons through DAT (21). MPTP injection eliminates more than 95% of DAT in striatal synaptosomes (Fig. 3B and C). MPTP reduces high-affinity [3 H]cocaine binding in striatal synaptosomes by about 30%. This corresponds well with the 40% reduction in BASP1 protein level in these samples but not to the 95% reduction in DAT levels (Fig. 3B–D). We compared diverse cocaine structural analogs/derivatives for their ability to elute [3 H]cocaine from BASP1-containing membranes. We evaluated compounds functionally related to cocaine, especially DAT inhibitors. While several DAT inhibitors displace cocaine from BASP1, others do not (Fig. 3E). Thus, inhibition of DAT transport activity is not a principal determinant of BASP1 binding. Out of 12 structural analogs, only benztropine and 3 β -(p-fluorobenzoyloxy)tropane (3-p-FBT) elute [3 H]cocaine from BASP1-containing membranes. Structurally similar compounds

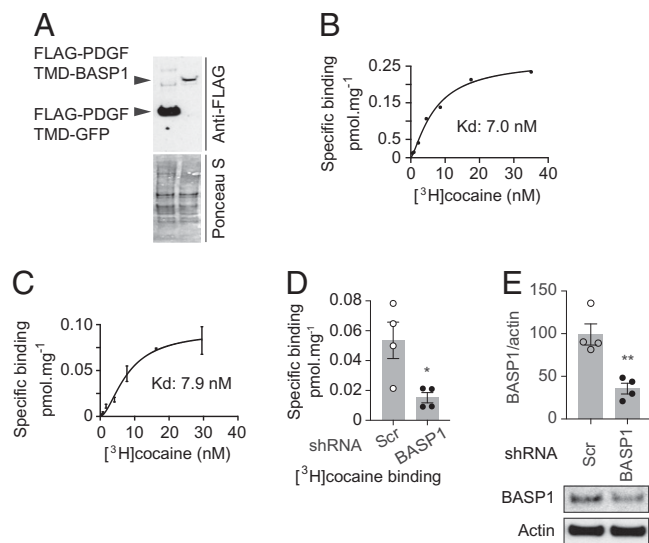


Fig. 2. High-affinity cocaine binding associated with BASP1. (A) Western blot analysis of membrane fractions isolated from HEK 293 cells' membrane fractions confirming the overexpression of FLAG-tagged PDGF transmembrane domain (FLAG-PDGF-TMD) fused to the N termini of GFP or BASP1. (B) Saturation binding curve for [3 H]cocaine and BASP1 overexpressed in HEK 293 cells and anchored to the membrane with a PDGF transmembrane domain. Membrane fraction is used for the saturation binding assay. K_d = 7.0 nM, R^2 = 0.99, specific binding with Hill slope. (C) Saturation binding curve for [3 H]cocaine to rat striatal synaptosome fraction. K_d = 7.9 nM, R^2 = 0.97, n = 2, error bars = \pm SD, specific binding with Hill slope. (D) AAV2-delivered shRNA to BASP1 reduces specific binding of [3 H]cocaine to mouse striatal synaptosome fraction. n = 4, $*P$ = 0.023, two-tailed t test. Error bars = \pm SEM. (E) Western blot of BASP1 in NAc preinjected with AAV2 that encodes scrambled (Scr) or BASP1 shRNA. The Westerns are for the same samples used in C. Quantification of Western blot band intensity of BASP1 normalized to actin is shown. n = 4, $**P$ = 0.0038, two-tailed t test. Error bars = \pm SEM.

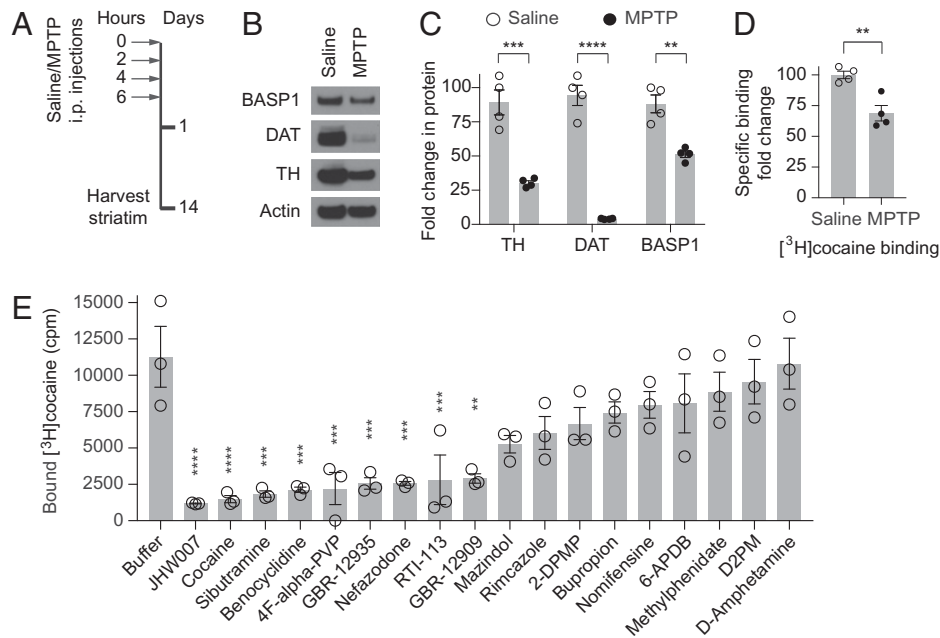


Fig. 3. Dopaminergic neurons contribution to high-affinity [³H]cocaine binding in the striatum. (A) Diagram showing the protocol of dopaminergic denervation of the striatum using a systemic injection of MPTP. (B) Western blot of BASP1, DAT, and TH in striatal synaptosomes isolated from mice treated with saline or MPTP. (C) Quantification of Western blot band intensity normalized to actin is shown. $n = 4$, $***P = 0.0007$, $****P < 0.0001$, $**P = 0.0018$, two-tailed t test. Error bars = \pm SEM. (D) Dopaminergic denervation reduces specific binding of [³H]cocaine (20 nM) to mouse striatal synaptosome fraction. $n = 4$, $***P = 0.0042$, two-tailed t test. Error bars = \pm SEM. (E) Specific binding of [³H]cocaine to membrane fraction of HEK 293 cells overexpressing BASP1 following elution with indicated compounds (10 μ M) related to cocaine. $n = 3$, one-way ANOVA, $P < 0.0001$, Bonferroni's multiple comparisons test, $****P < 0.0001$, $***P < 0.001$, $**P < 0.01$. Error bars = \pm SEM.

such as the major cocaine metabolite benzoylecgonine do not dissociate [³H]cocaine from BASP1 (*SI Appendix, Fig. S3 A and B*). These findings suggest that selective high-affinity cocaine binding is associated with BASP1.

BASP1 Mediates Locomotor Stimulation by Cocaine. We explored the influence of BASP1 depletion in NAc of intact mice utilizing shRNA incorporated into an adeno-associated virus (AAV2) (Fig. 4A). This shRNA treatment elicits a 50% depletion of BASP1 in NAc (Fig. 4B). We evaluated the effect of BASP1 depletion upon the behavioral effects of cocaine monitored as enhancement of horizontal locomotor activity by a single injection of cocaine (20 mg/kg) (Fig. 4 C–F) (22). BASP1 depletion without cocaine treatment does not affect the spontaneous locomotor activity of mice (Fig. 4 C–F). In control animals receiving scrambled shRNA, cocaine substantially enhances locomotor activity. BASP1 shRNA treatment reduces the stimulatory actions of cocaine by about 50% in male mice, which corresponds to a 50% reduction of endogenous BASP1 protein (Fig. 4 B–D). BASP1 depletion inhibits the cocaine-induced open field peripheral but not central locomotor activity in male mice (*SI Appendix, Fig. S4A*), suggesting that BASP1 regulates cocaine-induced hyperlocomotion but not voluntary exploration of unsafe areas. During the peak of cocaine-induced locomotor activity, BASP1 depletion prevents the reduction by cocaine of vertical/rearing activity in male mice (*SI Appendix, Fig. S4B*). In female mice, BASP1 shRNA treatment in NAc does not change the locomotor stimulatory actions of cocaine (Fig. 4 E and F and *SI Appendix, Fig. S4C*). We used an AAV2 vector, which undergoes retrograde transport along the axons of projection neurons. Hence, we confirmed the expression of GFP in the ventral midbrain following AAV2 injection in NAc (*SI Appendix, Fig. S4D*). To examine the specificity of influences of BASP1 shRNA treatment in NAc on cocaine-induced hyperlocomotion, we performed a rotarod

test in naïve male and female mice. Results from these experiments show no difference between the AAV2-BASP1-shRNA vs. AAV2-scrambled-shRNA groups (*SI Appendix, Fig. S4 E–G*).

We used AAV2-BASP1-shRNA to knock down BASP1 in the dorsal striatum of male and female mice (*SI Appendix, Fig. S4 H and I*). Mice injected with AAV2-BASP1-shRNA in the dorsal striatum do not show a difference in cocaine-induced locomotor activity compared to mice injected with AAV2-scrambled-shRNA (*SI Appendix, Fig. S4J*). The coordinates we used for viral infusions correspond to the posterior part of the dorsal striatum. It will be interesting to explore the effects of BASP1 in different regions of the dorsal striatum on cocaine-mediated behaviors. Our findings suggest that the depletion of BASP1 in the posterior dorsal striatum does not significantly regulate cocaine-induced locomotor activity.

Taken together, our findings suggest that BASP1 depletion in NAc inhibits cocaine-induced locomotor stimulation in male but not female mice.

Discussion

Our findings indicate that BASP1 (also known as NAP-22 and CAP-23) may be a pharmacologically relevant cocaine receptor. Thus, high-affinity binding (K_d of 7 nM) to [³H]cocaine in rodent striatum is associated with BASP1. Previous evidence demonstrates that dopamine signaling mediates the psychostimulant actions of cocaine (23). Several studies showed that eliminating dopaminergic terminals in the NAc abrogates the locomotor stimulant and rewarding effects of cocaine (17–20). Our findings show that dopaminergic denervation using MPTP leads to a 95% reduction of DAT levels in the striatum. Yet, [³H]cocaine binding to striatal synaptosomes is reduced by only 30%, resembling the 40% decrease in BASP1 protein level. These data suggest that dopaminergic terminals contribute a significant fraction (40%) of the BASP1 protein level in striatal synaptosomes.

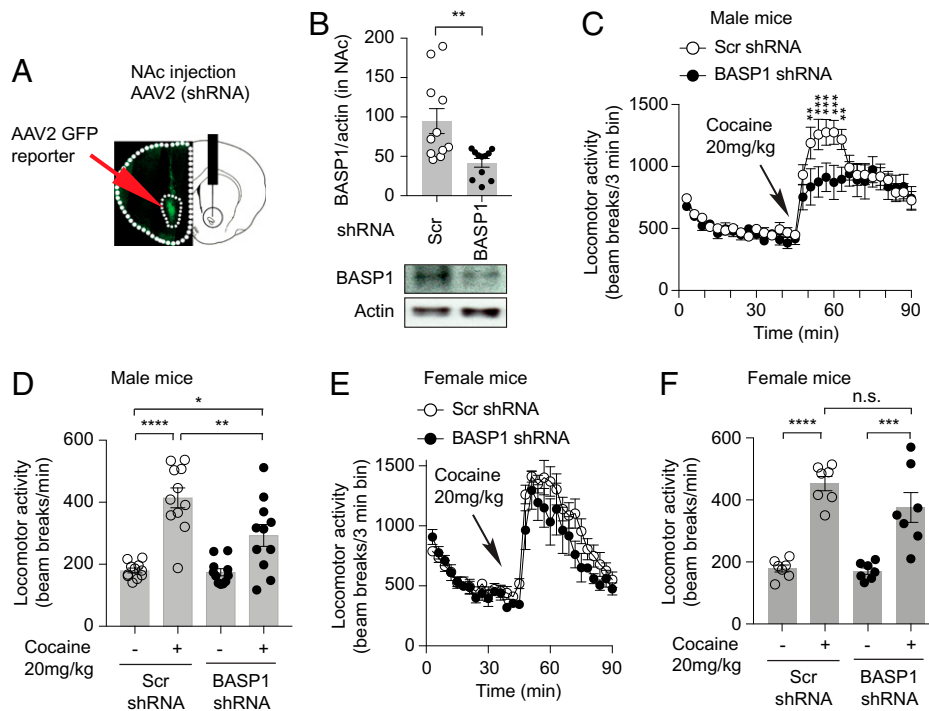


Fig. 4. BASP1 mediates the locomotor stimulant effect of cocaine. (A) GFP reporter confirmation of NAc targeting by stereotaxic injection. (B) Western blot of BASP1 in NAc preinjected with AAV2 that encodes scrambled (Scr) or BASP1 shRNA. The Westerns are from the same samples used in the behavioral assay (C and D). Quantification of Western blot band intensity of BASP1 normalized to actin is shown. $n = 11$ per group, $**P = 0.0048$, two-tailed t test. Error bars = \pm SEM. (C) Total locomotor activity of male mice in the open field test treated with cocaine preinjected with AAV2 scrambled (Scr) or BASP1 shRNA. $n = 11$ mice/group, two-way ANOVA, $**P = 0.0013$ and 0.0034 , respectively, $***P = 0.0005$, 0.0010 , and 0.0003 , respectively. Error bars = \pm SEM. (D) Peak locomotor activity of male mice in the open field test. $n = 11$ mice/group, one-way ANOVA, $P < 0.0001$, Bonferroni's multiple comparisons test, Scr shRNA group saline vs. cocaine treatment, $****P < 0.0001$, Scr shRNA + cocaine vs. BASP1 shRNA + cocaine, $**P = 0.0078$, Scr shRNA saline vs. BASP1 shRNA + cocaine, $*P = 0.015$. n.s. = not significant. Error bars = \pm SEM. (E) Total locomotor activity of female mice in the open field test treated with cocaine preinjected with AAV2 scrambled (Scr) or BASP1 shRNA. $n = 7$ mice/group. Error bars = \pm SEM. (F) Peak locomotor activity of female mice in the open field test. $n = 7$ mice/group, one-way ANOVA, $P < 0.0001$, Bonferroni's multiple comparisons test, Scr shRNA group saline vs. cocaine treatment, $****P < 0.0001$, BASP1 shRNA group saline vs. cocaine treatment, $***P = 0.0001$. Error bars = \pm SEM.

Further, our data suggest that one-third of the high-affinity [3 H]cocaine binding in striatal synaptosomes involves dopaminergic terminals. Other projection neurons to the striatum and resident striatal neurons, such as glutamatergic and medium spiny neurons, respectively, might contribute to the high-affinity [3 H]cocaine binding to striatal synaptosomes. Depleting endogenous BASP1 levels by 50% elicits a corresponding 50% decrease of [3 H]cocaine binding, suggesting that BASP1 accounts for all or the great majority of high-affinity [3 H]cocaine binding interactions in striatal synaptosomes.

To assess structural determinants of ligand binding to BASP1, we evaluated the ability of structural and functional cocaine analogs to displace cocaine from overexpressed BASP1. Of the structural cocaine analogs tested, only four (benztropine, 3-p-FBT, JHW007, and RTI-113) displaced cocaine from BASP1. Three of these drugs (benztropine, JHW007, and RTI-113) inhibit dopamine uptake (24–26). The pharmacology of the designer drug analog of cocaine 3-p-FBT has not been characterized (27). By contrast, tropane alkaloids, including benzocaine, atropine, and scopolamine, which lack dopamine uptake inhibitor activity, did not bind BASP1. Thus, our structure–activity relationship studies suggest that the BASP1 pharmacophore is not primarily determined by the tropane moiety of cocaine. Further, the lack of BASP1 binding by local anesthetic cocaine derivatives (benzocaine, procaine, and lidocaine) suggests that BASP1 is unlikely to mediate the local anesthetic effects of cocaine. Such actions have primarily been attributed to inhibition of sodium and potassium channels, actions that require levels of cocaine 1,000 times greater than those that bind BASP1 (28, 29).

The enhancement of locomotor activity by cocaine is reduced by depleting NAc BASP1 with shRNA in male but not female mice. Sex/gender-specific effects and the influences of ovarian hormones on the behavioral actions of cocaine are well documented. Sex/gender differences might be qualitative, quantitative, mechanistic, and/or population differences (30–32). It is not clear whether the differences we observed between male and female mice are due to gonadal hormone, chromosome, or epigenetic influences. It is also possible that circuit-based differences between males and females underlie these observations. An alternative explanation might be due to BASP1-mediated effect on axonogenesis, leading to decreased DA innervation in male but not female mice. However, we did not observe any reduction in DA neuron markers in the NAc following the knockdown of BASP1. These sex-specific differences might be related to estrogen and estrogen receptor modulatory effect on cocaine-induced hyperlocomotion in rodents (33–36). BASP1 appears to interact with and act as a transcriptional corepressor for the estrogen receptor in breast cancer cells (37). The interaction between BASP1 and estrogen signaling might explain sex-specific mediation of responses to cocaine. It will be interesting to determine whether BASP1 binds and regulates estrogen receptor signaling in the brain following cocaine administration.

Calligaro and Eldefrawi (3) reported a high-affinity [3 H]cocaine binding site in rat brain membranes whose properties resemble BASP1. BASP1 is a membrane-associated protein whose myristoylation links it to brain membranes. It is enriched in axon terminals and regulates neurite outgrowth, maturation of the actin cytoskeleton, and organization of the plasma membrane (12, 13, 38, 39). Its exact biochemical and behavioral functions have not heretofore

been elucidated. BASP1 is associated with cholesterol, a major component of lipid rafts in the brain (40). Some evidence suggests that BASP1 regulates the formation of lipid rafts (41, 42). Despite its small size, BASP1 induces cation-selective currents across negatively charged planar lipid bilayers (43).

BASP1 regulates many cellular signaling cascades, which have been implicated as modulators of the neurochemical and behavioral effects of cocaine. For example, BASP1 is phosphorylated by protein kinase C (PKC) and physiologically binds calmodulin (44, 45) as well as the calmodulin-dependent phosphatase calcineurin (46). Likewise, signaling through PKC and calcium/calmodulin-dependent protein kinase II is required for the rewarding effects of cocaine (47–52).

Modulation of the actin cytoskeleton is a key molecular mechanism underlying the plasticity of dendritic spines associated with cocaine abuse and reward (53, 54). BASP1 is functionally related to the growth-associated protein 43 (GAP-43), neuromodulin and the myristoylated alanine-rich C-kinase substrate (MARCKS), which are also enriched in presynaptic terminals. Specific interactions of GAP-43, MARCKS, and BASP1 with phospholipids and actin contribute to the regulation of neurotransmitter release, axonal growth cone guidance, and synaptic plasticity (22, 55).

BASP1 interacts physically and functionally with the histone deacetylase HDAC1 (16). While the exact roles of the diverse HDAC isoforms in cocaine actions remain unclear, HDACs have been implicated in transcriptional and behavioral responses to cocaine (56–59). It will be of interest to determine whether interactions of BASP1 with calcium/calmodulin, the actin cytoskeleton, and the histone-modifying machinery account for the influence of these systems on the neural and behavioral effects of cocaine.

BASP1 also has actions outside of the brain. For instance, in kidney-derived cells BASP1 binds to Wilms' tumor factor for which it serves as a transcriptional corepressor (15, 16). Furthermore, BASP1 seems to act as a tumor suppressor by inhibiting myc-induced oncogenesis (60). BASP1 may therefore warrant investigation as a mediator of peripheral actions of cocaine.

Previous literature demonstrates BASP1 enrichment in axon terminals (12, 13, 38, 39). Therefore, we anticipate BASP1 enrichment in the nerve endings of striatal medium spiny neurons and projection neurons to the striatum. Our findings suggest that 40% of BASP1 protein in the striatal synaptosomes is in dopaminergic terminals (Fig. 3 *A–D*). Our knockdown studies utilized an AAV vector, which undergoes retrograde transport along the axons of projection neurons (61–64). AAV viral particles have been detected in the soma of projection neurons as early as 24 h postinjection (61). Hence, our knockdown experiments are expected to affect both striatal and projection neurons. We have confirmed GFP reporter expression in the ventral mid-brain following AAV2 injection in NAc (*SI Appendix, Fig. S4D*). It will be interesting to determine the cellular effectors and circuit mechanisms underlying BASP1 regulation of cocaine signaling and behavioral actions.

Extensive evidence implicates inhibition of dopamine transport in the behavioral actions of cocaine (2, 65, 66). Cocaine fails to increase hyperlocomotion in DAT-deficient mice, establishing that DAT is necessary for cocaine-induced locomotor stimulation (67–69). Mice expressing low levels of DAT show enhanced hyperlocomotion after cocaine administration (70, 71). Cocaine-insensitive DAT knockin mice show inhibition of cocaine-induced locomotor activation, reward, and cocaine self-administration (10, 72, 73). However, several DAT inhibitors fail to produce cocaine-like effects in experienced human

volunteers (74, 75). We recently discovered that cocaine elicits neural autophagy with extraordinary potency (76). Inhibition of autophagy reduces the locomotor stimulant effect of cocaine, impairs cocaine conditioned place preference, and inhibits cocaine-elicited dopamine increase in NAc. Autophagy contributes to the cocaine-induced potentiation of dopaminergic neurotransmission through DAT degradation. Hence, the psychostimulant effects of cocaine involve autophagic degradation of DAT (76). To test whether BASP1 interacts with dopamine signaling, we monitored the impact of knocking down BASP1 in NAc on cocaine-induced DAT degradation. In this context, BASP1 knockdown inhibits cocaine-induced DAT depletion, which suggests that BASP1 mediates cocaine actions at least in part through dopamine reuptake inhibition via autophagic degradation of DAT. In this context it is likely that cocaine binding to BASP1 in dopaminergic terminals induces autophagy of DAT, which in turn contributes to the inhibition of dopamine reuptake. It will be interesting in future studies to define the molecular cascade linking cocaine binding to BASP1 and autophagic degradation of DAT.

In summary, BASP1 displays properties consistent with its serving as a cocaine receptor. Accordingly, drugs that disrupt BASP1–cocaine interaction might be useful as anticocaine medications.

Methods and Materials

Reagents. Neurobasal-A medium (no glucose, no sodium pyruvate), B-27 supplement, and B-27 supplement minus antioxidants were purchased from Life Technologies. Cocaine hydrochloride, atropine, benzoic acid, benzotropine, ecgonine, lidocaine, scopolamine, and glutathione agarose were purchased from Sigma-Aldrich. Anisodamine, benzocaine, benzoyllecgonine, benzotropine, 3-p-FBT (hydrochloride), procaine, and tropine were purchased from Cayman Chemical. Protein A/G PLUS-agarose was purchased from Santa Cruz Biotechnology. [³H]cocaine was purchased from PerkinElmer Life Sciences. FLAG-DAT plasmid (pchiygroflagsynhDAT) was a gift from Jonathan Javitch, Columbia University, New York, NY (Addgene plasmid #19990) (77). PDGF-TMD-GFP plasmid (pFU-no toxin-PE) was a gift from Ines Ibañez-Tallon, Rockefeller University, New York, NY (Addgene plasmid #24149) (78).

Cloning. A FLAG tag followed by the platelet-derived growth factor (PDGF) transmembrane domain (TMD) were cloned to the 5' end of BASP1, removing its ATG start codon to create a FLAG-PDGF-TMD-BASP1 fusion protein. *Bgl*I-*Asi*I restriction sites were used to insert the FLAG-PDGF-TMD fragment. The FLAG-PDGF-TMD fragment was derived from pFU-no toxin-PE Addgene plasmid #24149. The correct clone was identified by DNA sequencing to exclude any point mutants followed by overexpression in HEK 293 cells, isolation of the membrane fraction, and Western blot for the FLAG tag.

Antibodies. Anti-beta actin-horseradish peroxidase antibody was purchased from GeneScript, catalog no. A00730, clone 2D1D10, lot no. 13B000572 (79). Sheep anti-cocaine was purchased from US Biological Life Sciences, catalog no. C7505, lot no. L0031710A. Mouse anti-BASP1 (used in Fig. 3) was purchased from Santa Cruz Biotechnology, catalog no. sc-66994, clone H-100, lot no. B1715 (80, 81). Rabbit anti-BASP1 C-terminal region (used in Fig. 2) was purchased from Aviva Systems Biology, catalog no. ARP59932_P050, lot no. QC69877-43224. Rat anti-DAT was purchased from Santa Cruz Biotechnology, catalog no. sc-32258, clone 6-5G10, lot no. D0111 (82, 83). Rabbit anti-TH was purchased from BioLegend, catalog no. 818002 (84, 85). Mouse anti-FLAG antibody was purchased from Sigma Aldrich, catalog no. F3165, clone M2, lot number: SLBQ7119V (86, 87). Chicken anti-GFP was purchased from Abcam, catalog no. ab13970 (88, 89).

Animals. All experiments involving animals were conducted in accordance with the Johns Hopkins Medical Institution's Animal Care and Use Committee guidelines. C57BL/6j adult mice were purchased from The Jackson Laboratory. CD-1 timed pregnant mice and Sprague-Dawley male rats were purchased from

Charles River Laboratories. Animal handling and procedures were conducted in accordance with the NIH guidelines for the use of experimental animals and the Johns Hopkins animal care and use guidelines. For sample size determination, we used the sample size calculator at ClinCalc.com.

HEK 293 Cell Transfection. HEK 293 cells were transfected using the calcium phosphate method. Briefly, plasmid DNA was diluted in 2× Hepes-buffered saline buffer containing 1.5 mM disodium phosphate, 12 mM dextrose, 280 mM NaCl, 10 mM KCl, and 50 mM Hepes pH 7.05. Then, 0.25 M calcium chloride was added dropwise to the mix while vortexing on low speed. Transfection mixers were incubated at room temperature for 30 min then added to cells in a dropwise fashion. The medium was changed 24 h later. The cells were used 48 to 72 h after transfection.

Isolation of Membrane Fraction. HEK 293 cells were homogenized in buffer containing 0.25 M sucrose, 10 mM Hepes (pH 7.3), 1 mM ethylenediaminetetraacetic acid (EDTA), 0.5 μg/mL antipain, 1 μg/mL leupeptin, 1 μg/mL aprotinin, 1 μg/mL chymostatin, and 1 μg/mL pepstatin A. The homogenates were centrifuged at 1,000 × *g* for 10 min at 4 °C. The supernatants were centrifuged at 3,000 × *g* for 10 min at 4 °C. The supernatants from the last step were centrifuged at 10,000 × *g* for 10 min at 4 °C. Resultant supernatants were then loaded into a ultracentrifuge SW-55Ti rotor tube and spun at 100,000 × *g* for 1 h at 4 °C. Resulting pellets (membrane fractions) were resuspended in 10 mM sodium phosphate buffer (with 0.5 μg/mL antipain, 1 μg/mL leupeptin, 1 μg/mL aprotinin, 1 μg/mL chymostatin, and 1 μg/mL pepstatin A) to a concentration of ~0.5 mg/mL protein.

Cocaine IP. Cortical cultures were treated with 100 nM cocaine for 5 min, then washed in ice-cold phosphate buffered saline (PBS) and harvested on ice in IP buffer containing 10 mM sodium phosphate pH 7.2, 1% Nonidet P-40, 100 mM sodium chloride, 2 mM EDTA, 50 mM sodium fluoride, 200 μM sodium orthovanadate, 0.5 μg/mL antipain, 1 μg/mL leupeptin, 1 μg/mL aprotinin, 1 μg/mL chymostatin, and 1 μg/mL pepstatin A. Cell lysates were passed through a 27-gauge syringe 10 times, incubated on ice for 15 min, then cleared by centrifugation at 3,000 × *g* for 10 min at 4 °C. Equal amounts of total protein were incubated with sheep anti-cocaine antibody for 45 min at 4 °C with rotation. Then, protein A/G PLUS-agarose beads were added to the lysate-antibody mixture and rotated at 4 °C for 1 h. The beads were washed 5 times by a series of centrifugation (at 735 × *g*) and resuspension using tris-buffered saline buffer. Elution was performed using 10 nM cocaine. The eluates were then mixed with reducing sodium dodecyl sulfate (SDS)—loading buffer, boiled and separated by SDS—polyacrylamide gel electrophoresis or sent for mass spectrometric identification.

PCN Culture. Unless otherwise specified, PCNs were isolated from E16–E18 pregnant CD-1 mice. The pregnant mouse was killed by decapitation, then the uterus was dissected out immediately. Working in sterile conditions, the uterus was opened, the pups decapitated, and their brains dissected and placed in dissection media containing Dulbecco's modified Eagle's medium/F12 1:1 supplemented with 10% horse serum. The cerebral cortices were detached from the rest of the brain, and the meninges removed. The cortices were incubated in 0.025% trypsin for 15 min at 37 °C. The trypsin was washed with dissection media. The cortices were disrupted into single cell suspension by pipetting up and down 10 times, then strained through a 40-μm sterile mesh. The single cell suspension was cultured in dissection media overnight. Then the media were replaced by PCN plating media containing neurobasal-A medium (no glucose, no sodium pyruvate) supplemented with 12.5 mM glucose, 2 mM l-glutamine, and 2% B-27. On day 4 *in vitro* (DIV4) the media were changed to PCN maintenance media containing neurobasal-A medium (no glucose, no sodium pyruvate) + 12.5 mM glucose, 2 mM l-glutamine, and 2% B-27 minus antioxidants. Every third day thereafter, 50% of the media was replaced with PCN maintenance media.

Synaptosome Fraction Preparation. Crude synaptosome fractions were prepared as previously described (90) with minor modifications. Briefly, striata derived from male mice or rats were dissected and homogenized in a buffer containing 0.32 M sucrose, 20 mM Hepes (pH 7.4), 0.5 μg/mL antipain, 1 μg/mL leupeptin, 1 μg/mL aprotinin, 1 μg/mL chymostatin, and 1 μg/mL pepstatin A. The tissue homogenates were centrifuged at 3,000 × *g* for 10 min at 4 °C. The

supernatants were centrifuged at 10,000 × *g* for 15 min at 4 °C. The pellets (the crude synaptosome fraction) were resuspended in RIPA buffer (Cell Signaling Technology) containing 20 mM Tris-HCl (pH 7.5), 150 mM NaCl, 1 mM Na₂-EDTA, 1 mM ethylene glycol-bis(β-aminoethyl ether)-N,N,N',N'-tetraacetic acid, 1% Nonidet P-40, 1% sodium deoxycholate, 2.5 mM sodium pyrophosphate, 1 mM β-glycerophosphate, 1 mM Na₃VO₄, and 1 μg/mL leupeptin. The crude synaptosome fraction lysates were used for Western blot analysis. Western blot was performed following standard procedures except for the DAT experiments. For DAT Western blot analysis, samples were not boiled before loading into the gels. Instead, samples were heated at 52 °C for 30 min with shaking, then loaded into the gels.

Ligand Binding Assay. FLAG-tagged PDGF transmembrane domain fused to GFP on its N terminus (FLAG-TMD-GFP) or to BASP1 on its N terminus (FLAG-TMD-BASP1), or myc-FLAG fused to BASP1 on its C terminus (BASP1-myc-FLAG) were overexpressed in HEK 293 cells; enrichment at the membrane fraction was verified using subcellular fractionation and Western blot. Membrane fractions or striatal synaptosomal fractions were incubated with [³H]cocaine for 30 min at room temperature. Then the mixtures were passed through a polyethylenimine (PEI)-coated Whatman filter. The radioactivity retained on filters after four washes with ice-cold 150 mM NaCl was monitored using a scintillation counter (Beckman Coulter LS6500 Liquid Scintillation Counter with LS6500 software). Specific binding (total binding — binding in the presence of 100 μM unlabeled cocaine) was analyzed by curve fitting using nonlinear regression analysis in order to calculate the *K_d* and *B_{max}* of cocaine-BASP1 binding.

Dopaminergic Denervation. Dopaminergic denervation was performed as previously described (91). Briefly, mice were randomly allocated into two groups: saline or MPTP group. The mice were injected with four doses of MPTP (20 mg/kg, *i.p.* every 2 h) or saline and euthanized 14 d after the final saline or MPTP injection. Striata were dissected out and immediately processed for synaptosome isolation. Dopaminergic denervation was validated by Western blot analysis of DAT and tyrosine hydroxylase (TH) in striatal synaptosomes.

Stereotaxic Injection. Stereotaxic injections were performed as previously described with modifications (92). C57BL6/j mice (age range: 10 to 14 wk) were anesthetized with 125 mg/kg ketamine, 15 mg/kg xylazine, and 1.5 mg/kg acepromazine. A Stoelting's stereotaxic instrument for mice was used to perform the procedure. The skull was exposed, and burr holes were made at the stereotaxic coordinates specified below. The NAc was injected bilaterally using the following stereotaxic coordinates from bregma: +1.4 mm (anterior/posterior), ±1.3 mm (medial/lateral), and –4.3 mm (dorsal/ventral). One microliter of AAV2 was delivered on each side at a rate of 1 μL/min, followed by a 5-min pause at the site of injection, a 2-min pause at –3.3 (dorsal/ventral), and a 2-min pause at –2.3 (dorsal/ventral). For the striatal injections (for [³H]cocaine binding experiments), from bregma: –0.5 mm (anterior/posterior); ±2.0 mm (medial/lateral); 4 × 1 μL AAV2 injections were delivered on each side at a rate of 1 μL/min followed by a 2-min pause at the following depths: (dorsal/ventral) –4.5 mm (1 μL), –4.0 mm (1 μL), –3.5 mm (1 μL), and –3.0 mm (1 μL). Then, 5-min-long pauses were made at the following depths: (dorsal/ventral) –2.5 mm and –2.0 mm. For dorsal striatum injections, from bregma: +0.5 mm (anterior/posterior), 1.8 mm (medial/lateral), –2.5 (dorsal/ventral), and 1 μL AAV2 injections were delivered on each side at a rate of 1 μL/min followed by a 15-min pause in place (at –2.5). Then the needle was slowly removed. Confirmation of target sites was verified by visualizing GFP expression by confocal microscopy and qPCR of GFP. AAV2 encoding shRNA against BASP1 was purchased from Vector Biolabs; AAV2 encoding scrambled (Scr) shRNA was purchased from Vector Biolabs and the University of Iowa Viral Vector Core. Knockdown of BASP1 was verified by Western blot and qPCR. Western blot band intensities were quantified using NIH ImageJ 2.0.0.

Brain Tissue Processing. Mice were anesthetized with intraperitoneal injection of sodium pentobarbital (80 mg/kg). The thoracic cavity was exposed, and transcardiac perfusion was performed by inserting a needle to the left ventricle and puncturing the right atrium. PBS was used to start the perfusion for 5 min at a rate of 5 mL/min followed by ice cold 4% paraformaldehyde (PFA) in PBS for 30 min (using 3 mL/min rate). The brains were dissected and postfixed in 4% PFA for 24 h at 4 °C then cryoprotected with 30% sucrose in PBS for 24 h at

4 °C. Brains were sectioned on a freezing stage sliding microtome into a series of 40- μ m sections. A Zeiss LSM 800 confocal microscopy was used to image sections. ZEN imaging software (2.3 blue edition service pack 1, Carl Zeiss Microscopy), was used for data collection.

Mass Spectral Analysis.

Proteolysis. After adjusting pH to 8.0 with 4 μ L triethylammonium bicarbonate buffer, samples were reduced with 2 μ L \times 7.5 mg/mL dithiothreitol at 60 °C for 1 h, alkylated with 2 μ L \times 18.5 mg/mL iodoacetamide in the dark at room temperature for 15 min. Proteins were proteolyzed with 650 ng trypsin (lyophilized, Promega, <https://www.promega.com>) at 37 °C overnight. Tryptic peptides were desalted on Oasis u-HLB plates (Waters), then eluted with 65% acetonitrile/0.1% trifluoroacetic acid.

Liquid chromatography/tandem mass spectrometry analysis. Desalted tryptic peptides were analyzed by liquid chromatography/tandem mass spectrometry (LC-MS/MS) on nano-LC-QExactive HF in Fourier transform (Thermo Fisher Scientific, <http://www.thermofisher.com>) interfaced with the nano-Acquity LC system from Waters, using reverse-phase chromatography (2 to 90% acetonitrile/0.1% formic acid gradient over 75 min at 300 nL/min) on 75 μ m \times 150 mm ProntoSIL-120-5-C18 H column 5 μ m, 120 Å (Bischoff, <https://www.bischoff-chrom.com/hplc-prontosil-c18-h-c18-fasen.html>). Eluting peptides were sprayed into an QExactive HF mass spectrometer through a 1- μ m emitter tip (New Objective, <https://www.newobjective.com>) at 2.0 kV. Survey scans (full MSs) were acquired on an Orbi-trap within 350 to 1,800 Da *m/z* using a data-dependent top 15 method with dynamic exclusion of 16 s. Precursor ions were individually isolated with 1.6 Da, fragmented (MS/MS) using high-energy collisional dissociation activation collision energy 27 or 28. Precursor and the fragment ions were analyzed at resolution 120,000 automatic gain control (AGC) target 3×10^6 , max injection time (IT) 100 ms and 60,000, AGC target 1×10^5 , max IT 200 ms, respectively.

Data analysis. Tandem MS2 spectra were processed by Proteome Discoverer (v1.4 Thermo Fisher Scientific) in three ways, using 3Nodes: common, Xtract (spectra are extracted, charge state deconvoluted, and deisotoped using Xtract option, at resolution 95 K at 400 Da), MS2 Processor. MS/MS spectra from 3Nodes were analyzed with Mascot v.2.5.1 Matrix Science (<http://www.matrixscience.com>) specifying trypsin as enzyme, missed cleavage 2, precursor mass tolerance 8 ppm, fragment mass tolerance 0.015 Da, and oxidation (M), carbamidomethyl C, and deamidation NQ as variable modifications.

Open Field Test. Open field activity monitoring was performed in an open field Plexiglas chamber with photocell emitters and receptors to detect locomotor activity using a grid of invisible infrared beams (Photobeam Activity System, SDI PAS-Open Field software; San Diego Instruments). The chambers were enclosed in illuminated opaque boxes and connected to a computer for beam break data collection. Age-matched male mice preinjected in NAc with AAV2 encoding Scr or BASP1 shRNA (2 wk prior to experiment) were placed in the chambers for 45 min to detect baseline activity. After baseline monitoring, mice were given intraperitoneal injections of cocaine (20 mg/kg) or saline and returned to the chambers for 45 min to monitor their locomotor behavior. Cocaine's effect on peak locomotor activity was calculated based on the 15 min following cocaine injection. We measured the locomotor activity in the middle (central) vs. the

periphery (peripheral) of the open field arena to assess voluntary exploration of unsafe areas (the center of the open field).

Rotarod Test. The mice used in the rotarod test were naive male and female mice and did not undergo any other testing. The experiment was performed 2 wk following viral infusions into NAc. Data collection and analysis was performed blindly. We placed a soft padded surface at the base of the rotarod apparatus (Bioseb) to cushion mice that fall off. We conducted three trials separated by 15-min intertrial intervals performed during the dark phase of the 12-h light/12-h dark cycle for each mouse. The average time (latency) it took the mice to fall off the rod rotating under continuous acceleration (from 4 to 40 rpm) was recorded. Time was stopped when the mouse fell from the rod or after a 5-min limit. The mean speed at fall or at the end of 5 min was recorded.

Statistical Analysis. For sample size determination, we used the sample size calculator at ClinCalc.com: <https://clincalc.com/Stats/SampleSize.aspx>. Continuous endpoint, two independent sample study design was used with the following study parameters: probability of a type I error = 0.05, probability of a type II error = 0.1, power = 0.9. Statistical analysis was performed using Prism software (GraphPad Software, Inc.) with the alpha power level of 0.05. Unpaired *t* test was used to perform two group comparisons. Analysis of variance (ANOVA) was used to perform multiple comparisons followed by Bonferroni's multiple comparisons test. For ligand binding assays, curve fitting was performed using nonlinear regression analysis, specific binding with Hill slope. Unless otherwise indicated, data were graphed as means \pm SEM.

Data Availability All study data are included in the article and/or *SI Appendix*.

ACKNOWLEDGMENTS. We thank L. Hester, R. Barrow, A. Snowman, S. McTeer, and L. Albacarys from the S.H.S. laboratory for their assistance. We thank T. Boronina and the Mass Spectrometry Core at Johns Hopkins School of Medicine for helping with the mass spectrometry experiments. We are also grateful for fruitful discussions with L. Mario Amzel, Ph.D., Robert N. Cole, M.S., Ph.D., members of the S.H.S. laboratory, and Deiaa Harraz. This work was supported by US Public Health Service Grants DA00266 and DA044123 to S.H.S., DA044123 and NS38377 to T.M.D. and V.L.D., and a Brain and Behavior Research Foundation Young Investigator Grant (Grant 25360 to M.M.H.). T.M.D. is the Leonard and Madlyn Abramson Professor in Neurodegenerative Diseases.

Author affiliations: ^aThe Solomon H. Snyder Department of Neuroscience, Johns Hopkins University School of Medicine, Baltimore, MD 21205; ^bNeuroregeneration and Stem Cell Programs, Institute for Cell Engineering, Johns Hopkins University School of Medicine, Baltimore, MD 21205; ^cDepartment of Neurology, Johns Hopkins University School of Medicine, Baltimore, MD 21205; ^dDepartment of Pharmacology and Molecular Sciences, Johns Hopkins University School of Medicine, Baltimore, MD 21205; ^eDepartment of Physiology, Johns Hopkins University School of Medicine, Baltimore, MD 21205; and ^fDepartment of Psychiatry and Behavioral Sciences, Johns Hopkins University School of Medicine, Baltimore, MD 21205

Author contributions: M.M.H. conceived the original idea; M.M.H. and S.H.S. designed research; M.M.H., A.P.M., E.R.S., M. Shishikura, M. Singh, Y.H., I.G.K., Y.J.S., A.M.S., P.C., and S.S.K. performed research; T.M.D. and V.L.D. contributed new reagents/analytic tools; M.M.H., A.P.M., E.R.S., and Y.H. analyzed data; and M.M.H., E.R.S., and S.H.S. wrote the paper.

1. E. J. Nestler, The neurobiology of cocaine addiction. *Sci. Pract. Perspect.* **3**, 4–10 (2005).
2. F. S. Hall *et al.*, Molecular mechanisms underlying the rewarding effects of cocaine. *Ann. N. Y. Acad. Sci.* **1025**, 47–56 (2004).
3. D. O. Calligaro, M. E. Eldefrawi, Central and peripheral cocaine receptors. *J. Pharmacol. Exp. Ther.* **243**, 61–68 (1987).
4. C. S. Tallarida *et al.*, Ethanol and cocaine: Environmental place conditioning, stereotypy, and synergism in planarians. *Alcohol* **48**, 579–586 (2014).
5. L. Ferraro *et al.*, Nanomolar concentrations of cocaine enhance D2-like agonist-induced inhibition of the K⁺-evoked [3H]-dopamine efflux from rat striatal synaptosomes: A novel action of cocaine. *J. Neural Transm. (Vienna)* **117**, 593–597 (2010).
6. R. L. Strausberg, S. L. Schreiber, From knowing to controlling: A path from genomics to drugs using small molecule probes. *Science* **300**, 294–295 (2003).
7. J. Lamb *et al.*, The Connectivity Map: Using gene-expression signatures to connect small molecules, genes, and disease. *Science* **313**, 1929–1935 (2006).
8. P. Cuatrecasas, M. Wilchek, C. B. Anfinsen, Selective enzyme purification by affinity chromatography. *Proc. Natl. Acad. Sci. U.S.A.* **61**, 636–643 (1968).
9. R. Chen, D. D. Han, H. H. Gu, A triple mutation in the second transmembrane domain of mouse dopamine transporter markedly decreases sensitivity to cocaine and methylphenidate. *J. Neurochem.* **94**, 352–359 (2005).
10. R. Chen *et al.*, Abolished cocaine reward in mice with a cocaine-insensitive dopamine transporter. *Proc. Natl. Acad. Sci. U.S.A.* **103**, 9333–9338 (2006).
11. D. Mellacheruvu *et al.*, The CRAPome: A contaminant repository for affinity purification-mass spectrometry data. *Nat. Methods* **10**, 730–736 (2013).
12. F. Widmer, P. Caroni, Identification, localization, and primary structure of CAP-23, a particle-bound cytosolic protein of early development. *J. Cell Biol.* **111**, 3035–3047 (1990).
13. S. Maekawa, M. Maekawa, S. Hattori, S. Nakamura, Purification and molecular cloning of a novel acidic calmodulin binding protein from rat brain. *J. Biol. Chem.* **268**, 13703–13709 (1993).
14. D. Frey, T. Laux, L. Xu, C. Schneider, P. Caroni, Shared and unique roles of CAP23 and GAP43 in actin regulation, neurite outgrowth, and anatomical plasticity. *J. Cell Biol.* **149**, 1443–1454 (2000).
15. B. Carpenter *et al.*, BASP1 is a transcriptional cosuppressor for the Wilms' tumor suppressor protein WT1. *Mol. Cell Biol.* **24**, 537–549 (2004).
16. E. Toska *et al.*, Repression of transcription by WT1-BASP1 requires the myristoylation of BASP1 and the PIP2-dependent recruitment of histone deacetylase. *Cell Rep.* **2**, 462–469 (2012).
17. P. H. Kelly, S. D. Iversen, Selective 6OHDA-induced destruction of mesolimbic dopamine neurons: Abolition of psychostimulant-induced locomotor activity in rats. *Eur. J. Pharmacol.* **40**, 45–56 (1976).
18. K. A. Zito, G. Vickers, D. C. Roberts, Disruption of cocaine and heroin self-administration following kainic acid lesions of the nucleus accumbens. *Pharmacol. Biochem. Behav.* **23**, 1029–1036 (1985).
19. H. O. Pettit, A. Ettenberg, F. E. Bloom, G. F. Koob, Destruction of dopamine in the nucleus accumbens selectively attenuates cocaine but not heroin self-administration in rats. *Psychopharmacology (Berl.)* **84**, 167–173 (1984).
20. D. C. Roberts, G. F. Koob, Disruption of cocaine self-administration following 6-hydroxydopamine lesions of the ventral tegmental area in rats. *Pharmacol. Biochem. Behav.* **17**, 901–904 (1982).

21. J. A. Javitch, R. J. D'Amato, S. M. Strittmatter, S. H. Snyder, Parkinsonism-inducing neurotoxin, N-methyl-4-phenyl-1,2,3,6-tetrahydropyridine: Uptake of the metabolite N-methyl-4-phenylpyridine by dopamine neurons explains selective toxicity. *Proc. Natl. Acad. Sci. U.S.A.* **82**, 2173–2177 (1985).
22. Y. Itzhak, J. L. Martin, Effects of cocaine, nicotine, dizocipiline and alcohol on mice locomotor activity: Cocaine-alcohol cross-sensitization involves upregulation of striatal dopamine transporter binding sites. *Brain Res.* **818**, 204–211 (1999).
23. M. Xu *et al.*, Elimination of cocaine-induced hyperactivity and dopamine-mediated neurophysiological effects in dopamine D1 receptor mutant mice. *Cell* **79**, 945–955 (1994).
24. G. Tanda, A. H. Newman, J. L. Katz, Discovery of drugs to treat cocaine dependence: Behavioral and neurochemical effects of atypical dopamine transport inhibitors. *Adv. Pharmacol.* **57**, 253–289 (2009).
25. J. L. Katz, T. A. Kopajtic, G. E. Agoston, A. H. Newman, Effects of N-substituted analogs of benzotropine: Diminished cocaine-like effects in dopamine transporter ligands. *J. Pharmacol. Exp. Ther.* **309**, 650–660 (2004).
26. F. I. Carroll *et al.*, Cocaine and 3 beta-(4'-substituted phenyl)tropane-2 beta-carboxylic acid ester and amide analogues. New high-affinity and selective compounds for the dopamine transporter. *J. Med. Chem.* **38**, 379–388 (1995).
27. P. Kavanagh *et al.*, The syntheses and characterization 3β(4-fluorobenzyloxy)tropane (flurotropocaine) and its 3α isomer. *Drug Test. Anal.* **4**, 33–38 (2012).
28. J. C. Matthews, A. Collins, Interactions of cocaine and cocaine congeners with sodium channels. *Biochem. Pharmacol.* **32**, 455–460 (1983).
29. S. Ferreira, W. J. Crumb Jr., C. G. Carlton, C. W. Clarkson, Effects of cocaine and its major metabolites on the HERG-encoded potassium channel. *J. Pharmacol. Exp. Ther.* **299**, 220–226 (2001).
30. J. B. Becker, M. Hu, Sex differences in drug abuse. *Front. Neuroendocrinol.* **29**, 36–47 (2008).
31. M. E. Roth, K. P. Cosgrove, M. E. Carroll, Sex differences in the vulnerability to drug abuse: A review of preclinical studies. *Neurosci. Biobehav. Rev.* **28**, 533–546 (2004).
32. J. B. Becker, E. Chartoff, Sex differences in neural mechanisms mediating reward and addiction. *Neuropsychopharmacology* **26**, 479 (2018).
33. S. L. Sell, J. M. Scalzitti, M. L. Thomas, K. A. Cunningham, Influence of ovarian hormones and estrous cycle on the behavioral response to cocaine in female rats. *J. Pharmacol. Exp. Ther.* **293**, 879–886 (2000).
34. L. I. Perrotti *et al.*, Ovarian hormones modulate cocaine-induced locomotor and stereotypic activity. *Ann. N. Y. Acad. Sci.* **937**, 202–216 (2001).
35. D. Zhang, S. Yang, C. Yang, G. Jin, X. Zhen, Estrogen regulates responses of dopamine neurons in the ventral tegmental area to cocaine. *Psychopharmacology (Berl.)* **199**, 625–635 (2008).
36. S. A. M. Bobzean, T. S. Dennis, L. I. Perrotti, Acute estradiol treatment affects the expression of cocaine-induced conditioned place preference in ovariectomized female rats. *Brain Res. Bull.* **103**, 49–53 (2014).
37. L. A. Marsh *et al.*, BASP1 interacts with oestrogen receptor α and modifies the tamoxifen response. *Cell Death Dis.* **8**, e2771–e2771 (2017).
38. I. Korshunova *et al.*, Characterization of BASP1-mediated neurite outgrowth. *J. Neurosci. Res.* **86**, 2201–2213 (2008).
39. M. Matsubara, T. Nakatsu, H. Kato, H. Taniguchi, Crystal structure of a myristoylated CAP-23/NAP-22 N-terminal domain complexed with Ca²⁺/calmodulin. *EMBO J.* **23**, 712–718 (2004).
40. S. Maekawa *et al.*, Cholesterol-dependent localization of NAP-22 on a neuronal membrane microdomain (raft). *J. Biol. Chem.* **274**, 21369–21374 (1999).
41. R. M. Eppard, S. Maekawa, C. M. Yip, R. F. Eppard, Protein-induced formation of cholesterol-rich domains. *Biochemistry* **40**, 10514–10521 (2001).
42. R. F. Eppard, B. G. Sayer, R. M. Eppard, Induction of raft-like domains by a myristoylated NAP-22 peptide and its Tyr mutant. *FEBS J.* **272**, 1792–1803 (2005).
43. O. S. Ostroumova, L. V. Schagina, M. I. Mosevitsky, V. V. Zakharov, Ion channel activity of brain abundant protein BASP1 in planar lipid bilayers. *FEBS J.* **278**, 461–469 (2011).
44. A. Takasaki, N. Hayashi, M. Matsubara, E. Yamauchi, H. Taniguchi, Identification of the calmodulin-binding domain of neuron-specific protein kinase C substrate protein CAP-22/NAP-22. Direct involvement of protein myristoylation in calmodulin-target protein interaction. *J. Biol. Chem.* **274**, 11848–11853 (1999).
45. S. Maekawa, H. Murofushi, S. Nakamura, Inhibitory effect of calmodulin on phosphorylation of NAP-22 with protein kinase C. *J. Biol. Chem.* **269**, 19462–19465 (1994).
46. Y. Kobayashi *et al.*, Ganglioside contained in the neuronal tissue-enriched acidic protein of 22 kDa (NAP-22) fraction prepared from the detergent-resistant membrane microdomain of rat brain inhibits the phosphatase activity of calcineurin. *J. Neurosci. Res.* **93**, 1462–1470 (2015).
47. L. Cervo, S. Mukherjee, A. Bertaglia, R. Samanin, Protein kinases A and C are involved in the mechanisms underlying consolidation of cocaine place conditioning. *Brain Res.* **775**, 30–36 (1997).
48. A. J. Robison *et al.*, Behavioral and structural responses to chronic cocaine require a feedforward loop involving Δ FosB and calcium/calmodulin-dependent protein kinase II in the nucleus accumbens shell. *J. Neurosci.* **33**, 4295–4307 (2013).
49. H. D. Schmidt, R. L. Schassburger, L. A. Guercio, R. C. Pierce, Stimulation of mGluR5 in the accumbens shell promotes cocaine seeking by activating PKC gamma. *J. Neurosci.* **33**, 14160–14169 (2013).
50. A. C. Easton *et al.*, α CaMKII controls the establishment of cocaine's reinforcing effects in mice and humans. *Transl. Psychiatry* **4**, e457 (2014).
51. X. Liu *et al.*, CaMKII activity in the ventral tegmental area gates cocaine-induced synaptic plasticity in the nucleus accumbens. *Neuropsychopharmacology* **39**, 989–999 (2014).
52. L. A. Briand, A. U. Deutschmann, A. S. Ellis, A. Q. Fosnocht, Disrupting GluA2 phosphorylation potentiates reinstatement of cocaine seeking. *Neuropharmacology* **111**, 231–241 (2016).
53. S. Toda, H.-W. Shen, J. Peters, S. Cagle, P. W. Kalivas, Cocaine increases actin cycling: Effects in the reinstatement model of drug seeking. *J. Neurosci.* **26**, 1579–1587 (2006).
54. M. E. Cahill *et al.*, The dendritic spine morphogenic effects of repeated cocaine use occur through the regulation of serum response factor signaling. *Mol. Psychiatry* **23**, 1474–1486 (2018).
55. M. Hartl, R. Schneider, A unique family of neuronal signaling proteins implicated in oncogenesis and tumor suppression. *Front. Oncol.* **9**, 289 (2019).
56. A. Kumar *et al.*, Chromatin remodeling is a key mechanism underlying cocaine-induced plasticity in striatum. *Neuron* **48**, 303–314 (2005).
57. M. Malvaez, C. Sanchez-Segura, D. Vo, K. M. Lattal, M. A. Wood, Modulation of chromatin modification facilitates extinction of cocaine-induced conditioned place preference. *Biol. Psychiatry* **67**, 36–43 (2010).
58. P. J. Kennedy *et al.*, Class I HDAC inhibition blocks cocaine-induced plasticity by targeted changes in histone methylation. *Nat. Neurosci.* **16**, 434–440 (2013).
59. S.-Y. A. Tsai *et al.*, Sigma-1 receptor mediates cocaine-induced transcriptional regulation by recruiting chromatin-remodeling factors at the nuclear envelope. *Proc. Natl. Acad. Sci. U.S.A.* **112**, E6562–E6570 (2015).
60. M. Hartl, A. Nist, M. I. Khan, T. Valovka, K. Bister, Inhibition of Myc-induced cell transformation by brain acid-soluble protein 1 (BASP1). *Proc. Natl. Acad. Sci. U.S.A.* **106**, 5604–5609 (2009).
61. B. K. Kaspar *et al.*, Targeted retrograde gene delivery for neuronal protection. *Mol. Ther.* **5**, 50–56 (2002).
62. B. K. Kaspar, J. Lladó, N. Sherkat, J. D. Rothstein, F. H. Gage, Retrograde viral delivery of IGF-1 prolongs survival in a mouse ALS model. *Science* **301**, 839–842 (2003).
63. J. Fortun, R. Puzis, D. D. Pearce, F. H. Gage, M. B. Bunge, Muscle injection of AAV-NT3 promotes anatomical reorganization of CST axons and improves behavioral outcome following SCI. *J. Neurotrauma* **26**, 941–953 (2009).
64. J. H. Jara, S. R. Villa, N. A. Khan, M. C. Bohn, P. H. Ozdinler, AAV2 mediated retrograde transduction of corticospinal motor neurons reveals initial and selective apical dendrite degeneration in ALS. *Neurobiol. Dis.* **47**, 174–183 (2012).
65. S. Izenwasser, The role of the dopamine transporter in cocaine abuse. *Neurotox. Res.* **6**, 379–383 (2004).
66. K. C. Schmitt, M. E. A. Reith, Regulation of the dopamine transporter: Aspects relevant to psychostimulant drugs of abuse. *Ann. N. Y. Acad. Sci.* **1187**, 316–340 (2010).
67. B. Giros, M. Jaber, S. R. Jones, R. M. Wightman, M. G. Caron, Hyperlocomotion and indifference to cocaine and amphetamine in mice lacking the dopamine transporter. *Nature* **379**, 606–612 (1996).
68. I. Sora *et al.*, Cocaine reward models: Conditioned place preference can be established in dopamine- and in serotonin-transporter knockout mice. *Proc. Natl. Acad. Sci. U.S.A.* **95**, 7699–7704 (1998).
69. I. Sora *et al.*, Molecular mechanisms of cocaine reward: Combined dopamine and serotonin transporter knockouts eliminate cocaine place preference. *Proc. Natl. Acad. Sci. U.S.A.* **98**, 5300–5305 (2001).
70. A. Rao, A. Sorokin, N. R. Zahniser, Mice expressing markedly reduced striatal dopamine transporters exhibit increased locomotor activity, dopamine uptake turnover rate, and cocaine responsiveness. *Synapse* **67**, 668–677 (2013).
71. M. R. Tilley *et al.*, Cocaine reward and locomotion stimulation in mice with reduced dopamine transporter expression. *BMC Neurosci.* **8**, 42–47 (2007).
72. H. Wu *et al.*, Restoration of cocaine stimulation and reward by reintroducing wild type dopamine transporter in adult knock-in mice with a cocaine-insensitive dopamine transporter. *Neuropharmacology* **86**, 31–37 (2014).
73. M. Thomsen, D. D. Han, H. H. Gu, S. B. Caine, Lack of cocaine self-administration in mice expressing a cocaine-insensitive dopamine transporter. *J. Pharmacol. Exp. Ther.* **331**, 204–211 (2009).
74. L. D. Chait, E. H. Uhlenhuth, C. E. Johanson, Reinforcing and subjective effects of several anorectics in normal human volunteers. *J. Pharmacol. Exp. Ther.* **242**, 777–783 (1987).
75. K. A. Schoedel, D. Meier, B. Chakraborty, P. M. Marniche, E. M. Sellers, Subjective and objective effects of the novel triple reuptake inhibitor tesofensine in recreational stimulant users. *Clin. Pharmacol. Ther.* **88**, 69–78 (2010).
76. M. M. Harraz *et al.*, Cocaine-induced locomotor stimulation involves autophagic degradation of the dopamine transporter. *Mol. Psychiatry* **26**, 370–382 (2021).
77. C. Saunders *et al.*, Amphetamine-induced loss of human dopamine transporter activity: An internalization-dependent and cocaine-sensitive mechanism. *Proc. Natl. Acad. Sci. U.S.A.* **97**, 6850–6855 (2000).
78. S. Auer *et al.*, Silencing neurotransmission with membrane-tethered toxins. *Nat. Methods* **7**, 229–236 (2010).
79. I. Lee *et al.*, Membrane adhesion dictates Golgi stacking and cisternal morphology. *Proc. Natl. Acad. Sci. U.S.A.* **111**, 1849–1854 (2014).
80. R. M. Eppard, P. Vuong, C. M. Yip, S. Maekawa, R. F. Eppard, Cholesterol-dependent partitioning of PtdIns(4,5)P₂ into membrane domains by the N-terminal fragment of NAP-22 (neuronal axonal myristoylated membrane protein of 22 kDa). *Biochem. J.* **379**, 527–532 (2004).
81. S. Iino, K. Taguchi, S. Maekawa, Y. Nojyo, Motor, sensory and autonomic nerve terminals containing NAP-22 immunoreactivity in the rat muscle. *Brain Res.* **1002**, 142–150 (2004).
82. M. Di Salvio *et al.*, Otx2 controls neuron subtype identity in ventral tegmental area and antagonizes vulnerability to MPTP. *Nat. Neurosci.* **13**, 1481–1488 (2010).
83. K. N. Cameron, E. Solis Jr., I. Ruchala, L. J. De Felice, J. M. Eltit, Amphetamine activates calcium channels through dopamine transporter-mediated depolarization. *Cell Calcium* **58**, 457–466 (2015).
84. P. Marfull-Oromí *et al.*, Genetic ablation of the Rho GTPase Rnd3 triggers developmental defects in internal capsule and the globus pallidus formation. *J. Neurochem.* **158**, 197–216 (2021).
85. L. Shi *et al.*, Acroline scavenger dimeric caprol forms neuroprotection in an animal model of Parkinson's disease: Implication of acroline and TRPA1. *Transl. Neurodegener.* **10**, 13–15 (2021).
86. S. Oku, N. Takahashi, Y. Fukata, M. Fukata, In silico screening for palmitoyl substrates reveals a role for DHHC1/3/10 (zDHHC1/3/11)-mediated neurocholesterol palmitoylation in its targeting to Rab5-positive endosomes. *J. Biol. Chem.* **288**, 19816–19829 (2013).
87. N. Martin *et al.*, Interplay between Homeobox proteins and Polycomb repressive complexes in p16INK^a regulation. *EMBO J.* **32**, 982–995 (2013).
88. B. Schürmann *et al.*, A novel role for the late-onset Alzheimer's disease (LOAD)-associated protein Bin1 in regulating postsynaptic trafficking and glutamatergic signaling. *Mol. Psychiatry* **25**, 2000–2016 (2020).
89. M. B. Krawchuk, C. F. Ruff, X. Yang, S. E. Ross, A. L. Vazquez, Optogenetic assessment of VIP, PV, SOM and NOS inhibitory neuron activity and cerebral blood flow regulation in mouse somatosensory cortex. *J. Cereb. Blood Flow Metab.* **40**, 1427–1440 (2020).
90. M. M. Harraz, R. Tyagi, P. Cortés, S. H. Snyder, Antidepressant action of ketamine via mTOR is mediated by inhibition of nitergic Rheb degradation. *Mol. Psychiatry* **21**, 313–319 (2016).
91. S. S. Kruppagounder *et al.*, The c-Abl inhibitor, nilotinib, protects dopaminergic neurons in a preclinical animal model of Parkinson's disease. *Sci. Rep.* **4**, 4874–4878 (2014).
92. M. M. Harraz, S. M. Eacker, X. Wang, T. M. Dawson, V. L. Dawson, MicroRNA-223 is neuroprotective by targeting glutamate receptors. *Proc. Natl. Acad. Sci. U.S.A.* **109**, 18962–18967 (2012).